Spatial Variability and the Fate of Cesium in Coastal Sediments near Fukushima, Japan

E.E. Black and K.O. Buesseler

Woods Hole Oceanographic Institution
266 Woods Hole Road, Mail Stop #25, Woods Hole, MA 02543-1050 U.S.A.

Correspondence to: E.E. Black (eblack@whoi.edu) and K.O. Buesseler (kbuesseler@whoi.edu)

Abstract. Quantifying the amount of cesium incorporated into marine sediments as a result of the Fukushima Dai-ichi Nuclear Power Plant (FDNPP) accident has proven challenging due to the limited multi-core sampling from within the 30 kilometer zone around the facility, the inherent spatial heterogeneities in ocean sediments, and the potential for inventory fluctuations due to physical, biological, and chemical processes. Using ^{210}Pb, ^{234}Th, ^{137}Cs, and ^{134}Cs profiles from 20 sediment cores, coastal sediment inventories were reevaluated. A ^{137}Cs sediment inventory of 100 ± 50 TBq was found for an area of 55,000 km^2 using cores from this study and a total of 130 ± 60 TBq using an additional 181 samples. These inventories represent less than 1% of the estimated 15-30 PBq of cesium released during the FDNPP disaster. The time needed for surface sediment activities (0 to 3 cm) at the 20 locations to be reduced by 50% via sediment mixing was estimated to range from 0.4 to 26 years. Due to the observed variability in mixing rates, grain size, and inventories, additional cores are needed to improve these estimates and capture the full extent of cesium penetration into the shallow coastal sediments, which was deeper than 14 cm for all cores retrieved from water depths less than 150 m.

1 Introduction

The Tohoku earthquake and tsunami of 11 March 2011 led to multiple system failures at the Fukushima Dai-ichi Nuclear Power Plant (FDNPP). Over the next month, cooling water releases and hydrogen explosions resulted in the largest nuclear disaster since Chernobyl. Oceanic inputs included direct cooling discharge, runoff, riverine flow, and an estimated 70 to 80% of the total atmospheric radionuclide release (Aoyama et al., 2012). While later reports indicate additional releases to the ocean (TEPCO, 2014; Kanda, 2013), the initial ^{137}Cs activities measured in the FDNPP discharge channel from March to May of 2011 represent the most significant oceanic contribution to date, peaking at 68 million Bq m^{-3} on April 6th 2011 (Buesseler et al., 2011). ^{137}Cs emerged as the major oceanic contaminant warranting long-term study due to its ~30 year half-life and large release, generally estimated to be around 15 - 30 PBq (Buesseler, 2014; Charette et al., 2013; Povinec et al., 2013; Chino et al., 2011; Stohl et al., 2011). ^{137}Cs and ^{134}Cs (t½ ~2 years) have been found with comparable activities near the FDNPP and were released with a ratio of ~1 (Buesseler et al., 2011). Although the isotopes are highly soluble in the coastal ocean (Buesseler et al., 2012), a small percentage of the release will have been incorporated into the marine sediments and may remain associated with the seafloor, even after currents transport much of the dissolved phase away from the coast. Initial studies of the sediments near the FDNPP have shown the widespread incorporation of ^{137}Cs well above the relatively small remaining 1960's fallout signal of 1- 2 Bq kg^{-1} (dry) (NRA, 2014b; Kusakabe et al., 2013; Otosaka and Kato, 2014; Otosaka and Kobayashi, 2013).

The most spatially and temporally extensive sediment datasets have been provided by the Ministry of Education, Culture, Sports, Science and Technology-Japan (MEXT) and the Tokyo Electric Power Company (TEPCO). TEPCO initially reported some of the highest ^{134}Cs sediment activities in July of 2011 (TEPCO station 1 at 9600 Bq kg^{-1} wet) in grab samples collected within the 30 km zone around FDNPP (NRA, 2014a). However, lacking bulk density measurements, inventory estimates have not been published for this region. MEXT, on the other hand, reported monthly multi-corer, dry activities for homogenized 0 to 3 cm core tops from outside the 30 km zone (NRA, 2014b). Kusakabe et al. (2013) used 30 different MEXT locations ranging from 45 to 675 m water depth to estimate a ^{137}Cs sediment inventory of 38 TBq for the top 3 cm. As both datasets are limited to the uppermost layers of the sediment column, calculations using only these measurements will underestimate the total incorporation of

cesium into the sediments. In a more recent effort, Otosaka and Kato (2014) paired MEXT cores with 10 cm Smith-McIntyre grab samples and sectioned cores ranging from 3 to 10 cm and estimated a ^{134}Cs coastal inventory of 200 ± 60 TBq, decay-corrected to March 2011.

Larger datasets are essential for more accurate sediment inventory calculations due to the spatial variability and local heterogeneity observed in previous coastal sediment studies from this region (Kusakabe et al., 2013; Thornton et al., 2013). Kusakabe et al. (2013) found a ^{137}Cs activity range of 170 to 580 Bq kg^{-1} with six successive multi-corer casts at nominally the same sampling site (mean and standard deviation of 330 ± 160 Bq kg^{-1} dry). In addition, Thornton et al. (2013) reported activity fluctuations of <10 to 1500 Bq kg^{-1} at sites located between 5 and 10 km of the FDNPP and from 500 to 40,000 Bq kg^{-1} within 3 km of the FDNPP. These local anomalies were observed over distances of less than 1 km using a continuous (1 hertz) towed gamma ray spectrometer and their magnitude illustrates the importance of high spatial resolution sampling.

The evolution and ultimate fate of cesium isotopes in the coastal ocean must be better constrained to assess both the short term implications of the FDNPP accident and the potential for lasting effects. Reports that bottom water fish contain higher cesium concentrations than pelagic fish suggest that the sediments could be a continued source to bottom-dwelling biota (Buesseler, 2012). A model study of the coastal food chain near Fukushima indicated that an additional contamination source beyond ocean water, mostly likely associated with the sediments, would be necessary to sustain the cesium levels observed in higher trophic organisms (Tateda et al., 2013).

^{210}Pb (t ½ ~ 22.2 years) and ^{234}Th (t ½ ~ 24 days), naturally occurring daughter products in the ^{238}U decay series, can aid in evaluating the rates of sedimentation and bioturbation occurring in sediments from months to decades (Yang et al., 1985). ^{234}Th is particle reactive and will be scavenged easily in the upper ocean, leading to a potential excess in sediments (^{234}Th$_{ex}$). Because of its short half-life, measureable ^{234}Th$_{ex}$ is generally only observed in the top few cm of the sediment column in areas of rapid and recent mixing. Excess ^{210}Pb (^{210}Pb$_{ex}$) is supplied via atmospheric deposition, from the decay of ^{222}Rn gas, and scavenging in the water column. In sediments ^{210}Pb$_{ex}$ represents the divergence from secular equilibrium with ^{226}Ra (supported ^{210}Pb). If conditions are relatively stable, the ^{210}Pb$_{ex}$ inventory in a given area will represent the flux to this location averaged over the last century (~5 half-lives).

2 Methods

2.1 Sample Collection

Twenty sediment cores ranging in length from 6 to 20 cm were collected during cruise campaigns in May 2012 (R/V Tansei Maru), June and July 2012 (R/V Mirai), May 2013 (R/V Umitaka Maru), and September 2013 (R/V Daisan Kaiyo Maru). Stations were located 2 to 1,865 km from the FDNPP (Supplement S1). Individual core tubes were retrieved from a multi-corer and cross-sectioned at sea into 0.5 to 2 cm layers. A sample (plug) of 1 or 7 cm^3 was taken from each layer as the cores were cross-sectioned for density calculations. Sediment layers were preserved in sealed bags and the plug samples in capped vials. Eight samples (0 to 5 cm) from separate core tubes (R1 to R8) were retrieved from a single cast at the location of core 13 for an analysis of local variability.

2.2 Grain Size Analysis

Grain size analysis was performed on a subset of ~3 cm^3 core samples using a Beckman Coulter LS13320 particle size analyzer with capabilities of 0.4 µm to 2 mm. Grain size results are reported as percent clay and percent fines (silt plus clay) averaged over the entire depth of each core. Percent clay and percent fines were calculated by summing the frequency outputs from 0 to 3.86 µm and from 0 to 63.41 µm, respectively. D50 values were determined, which signify the grain size at which 50% of the sample is smaller or larger by particle count. All grain average size results are reported with standard deviations. Samples from cores 15 and 16 consisted of up to 42% of grains over 1 mm by mass and were processed differently due to the counter limitations. To ensure that no prolate grains with a near 2 mm axis passed to the counter, a 1 mm sieve was placed over the sample delivery system. The total mass of sample used, ranging from 5 to 45 grams, was determined by the counter's optimal obscuration range or percentage of light blockage by grains (15 to 25%).

2.3 Isotope Measurements

Samples were dried at 40-60 °C for a minimum of 1 day and analyzed using Canberra GCW4030S germanium gamma well detectors for the following energy peaks: 46.5 keV (^{210}Pb),

63.3 keV (^{234}Th), 352 keV (^{214}Pb), 661 keV (^{137}Cs), 795 keV (^{134}Cs). Samples were counted for 7 to 24 hours depending on the time to achieve counting uncertainties of less than 5% on the primary peaks. Detectors were calibrated using a dilute pitchblende ore standard (US EPA Environmental Monitoring Systems Lab) and river sediment standard (NBS 4350 B). Minimum detectable activities (MDAs) were calculated using 24 hour background spectra and efficiencies based on the average sample mass of 16.75 grams and sample volume of 14.5 mL (Currie, 1968). The calculated MDAs in Bq kg^{-1} were 4.2 (^{210}Pb), 3.2 (^{234}Th), 0.7 (^{214}Pb), 0.4 (^{137}Cs), and 0.8 (^{134}Cs). Activities under the MDAs and those with counting uncertainties over 50% were reported as not detectable (ND). Total uncertainties for a given sample and isotope (in Bq kg^{-1} dry) represent the higher of either the counting uncertainty or 7%. The minimum uncertainty (7%) is the average percent difference between sample activity results when duplicate measurements were made using the same and different detectors. The total uncertainty is propagated through all activity and inventory calculations for individual sections and full cores.

^{210}Pb activities were decay-corrected to the collection date and adjusted for supported values from ^{214}Pb (assumed to be at equilibrium with parent ^{226}Ra) to determine $^{210}Pb_{ex}$. Since an excess of ^{234}Th generally exists only in the first few cm, an estimation of equilibrium ^{234}Th values at depth were used to determine $^{234}Th_{supported}$, the activity supported by the decay of its ^{238}U parent, to calculate $^{234}Th_{ex}$ (decay-corrected to collection). All ^{134}Cs and ^{137}Cs data were decay-corrected to the date of maximum concentrations at the FDNPP (6 April, 2011; Buesseler et al., 2011). By decay-correcting, the changes we observe can be attributed to physical and biological processes and not radioactive decay. All final $^{210}Pb_{ex}$, $^{234}Th_{ex}$, and cesium activities for an individual layer are reported as Bq kg^{-1} dry and surface activities were calculated as the weighted (relative to layer thickness) average of layer activities for the top 3 cm of each core.

Layer inventories in Bq m^{-2} were calculated for ^{134}Cs, ^{137}Cs, $^{210}Pb_{ex}$, and $^{234}Th_{ex}$ using the following relationship:

$$Inventory = Layer\ Thickness * Bulk\ Density * Activity \quad (1)$$

where layer thickness was in meters, activities were in Bq kg^{-1} dry, and bulk density (kg m^{-3}) was equal to the amount of dry mass of sample in the 1 or 7 cm^3 plug divided by the total volume. All layer inventories for each isotope were summed to calculate total inventories for each

individual core except for $^{234}Th_{ex}$, which was only reported for the exponentially decreasing surface activities. Because core lengths ranged from 6 to 20 cm, some core inventories would not be representative of the complete isotope profile at that location if $^{210}Pb_{ex}$ values remain elevated at depth.

We estimated the expected sediment inventories of $^{210}Pb_{ex}$ in the coastal sediments near Fukushima, Japan using an average $^{210}Pb_{ex}$ atmospheric delivery flux of approximately 200 Bq $m^{-2} \cdot yr^{-1}$ to obtain an expected inventory from atmospheric input of 6400 Bq m^{-2} ($200 * 32$ years, mean life of ^{210}Pb). The atmospheric delivery flux estimate was derived from average monthly ^{210}Pb deposition measurements from 1993 to 2001 for Tokai-Mura (Ueno et al., 2003) and from 2000 to 2001 for Tokyo and Sendai (Yamamoto et al., 2006). Since ^{210}Pb is particle reactive, in-situ scavenging provides an additional source, the strength of which is a function of the ^{210}Pb:^{226}Ra disequilibrium, and water depth over which the deficit is found. Since we do not have ^{210}Pb:^{226}Ra profiles, we can only estimate a rough scavenging flux for ^{210}Pb using a Pacific $^{210}Pb/^{226}Ra$ ratio of 0.75 (Tsunogai and Harada, 1980) with a deep sea ^{226}Ra of approximately 33 dpm per 100 kg activity (28.5°N and 145°E; Nozaki and Tsunogai, 1976). This flux would be a linear function of water depth over which the disequilibrium applies, and ranges from 70 to 7,000 Bq m^{-2} for depths of 50 m to 5000 m (1-D scavenging supply equal to ^{226}Ra-$^{210}Pb * \lambda * z *$ 32 years). Thus, in most coastal settings, the dominant supply of ^{210}Pb is atmospheric deposition, whereas inventories are expected to increase with depth in the shelf and slope due to scavenging processes in the water column above. In addition, with a relatively long residence time for scavenging, ocean margins in general are sites of enhanced boundary scavenging of ^{210}Pb (Cochran et al., 1990).

2.4 Modeling

While the mixing of marine sediments often occurs via spatially and temporally variable bioturbation processes, such as non-local transport, the cumulative result of sediment accumulation, mixing, and isotope decay is often modeled as a diffusive process and can be written:

$$\frac{\partial}{\partial t}\{\rho(1-\phi) * A\} = \frac{\partial}{\partial x}\left\{D_B \rho(1-\phi)\frac{\partial A}{\partial x}\right\} - \frac{\partial}{\partial x}\{\rho(1-\phi)w * A\} + \rho(1-\phi)\lambda A \quad (2)$$

where ρ represents density, A activity of radionuclide, t time, w sedimentation rate, and λ represents the decay constant (Cochran, 1985). To generate mixing rates (D_B) using this relationship for each core, steady state, constant porosity (ϕ), and constant D_B with depth (x) were assumed. Equation (2) can be simplified using these assumptions to:

$$Activity = A_o e^{\frac{w-\sqrt{w^2-4D_B\lambda}}{2D_B}\cdot z} \quad (3)$$

where A_o is the activity at $x = 0$ (Anderson et al., 1988). Sedimentation can be ignored if:

$$w^2 \ll 4D_B\lambda \quad (4)$$

Historical $^{210}Pb_{ex}$-derived mixing rates from locations in the northwestern Pacific for depths greater than 4000 m range from 0.1 to 1 $cm^2\ yr^{-1}$ (Moon et al., 2003; Yang et al., 1985). Sedimentation rates for these locations were found to be 0.0001 to 0.002 cm yr^{-1}. Using the offshore mixing rates as a minimum for the coastal region near Fukushima, w would need to approach 0.12 cm yr^{-1} to be considered significant. Therefore, sedimentation was considered negligible over the decades following the FDNPP release and Eq. (2) can be further simplified to (Cochran, 1985; Yang et al., 1985):

$$Activity = A_o e^{-x\sqrt{\frac{\lambda}{D_B}}} \quad (5)$$

A dynamic, exponential regression analysis was performed on $^{234}Th_{ex}$ and $^{210}Pb_{ex}$ activity (Bq kg^{-1} dry) profile sections of each core using Eq. (5). In practice, mixing rates are typically higher in surface sediments and therefore $^{234}Th_{ex}$ profiles were used to derive D_B for upper layers, when present, and $^{210}Pb_{ex}$ was used below. Bioturbation was assumed to be the dominate process controlling isotope distributions in the sediments although D_B is a diffusive approximation of the combined effect of bioturbation and potential physical mixing processes.

To model the expected changes over time in ^{137}Cs profiles we used a pulse input model and the $^{234}Th_{ex}$- and $^{210}Pb_{ex}$-derived D_Bs (Cochran, 1985; Yang et al., 1985):

$$\frac{A}{A_o} = e^{\frac{-z^2}{4D_B t}} \quad (6)$$

where A is the activity at any given depth z, A_o is the shallowest surface activity, D_B is the mixing rate, and t is the time since the maximum input (6 April 2011; Buesseler et al., 2011). Keeping all other variables constant, we modeled the cesium activity profiles to determine the time needed for average cesium activities from the top 3 cm to decrease by 50% due to sediment mixing and hence, the transport of the cesium deeper into the core. Therefore, we have assumed that most of the cesium input to the sediments would track cesium delivery to the coastal waters. Sediment trap data in the north Pacific show rapid transport of cesium to depth, even in deep waters, within days of the input of cesium to the surface ocean (Honda et al., 2013).

3 Results and Discussion

3.1 Variability Between Multi-Core Tubes

From a single multi-corer cast, we retrieved 8 separate sample tubes (R1 to R8) and analyzed each for $^{210}Pb_{ex}$, ^{137}Cs, and ^{134}Cs. Core 13 was retrieved from the same location during an additional mutli-corer cast (Fig. 1). ^{137}Cs activities in the top 0 to 5 cm of these subcores varied from 45 ± 3 to 220 ± 20 Bq kg^{-1} and $^{210}Pb_{ex}$ from 140 ± 10 to 220 ± 20 Bq kg^{-1} (Supplement S2). Inventories for ^{137}Cs in the top 5 cm were 1600 ± 100 to 6500 ± 500 Bq m^{-2} and 5500 ± 400 to 7800 ± 600 Bq m^{-2} for $^{210}Pb_{ex}$. Inventories for core 13 for the same 0 to 5 cm layer were 8000 ± 200 and 6400 ± 200 Bq m^{-2} for ^{137}Cs and $^{210}Pb_{ex,}$ respectively. The large inventory differences for both ^{137}Cs and $^{210}Pb_{ex}$ indicate a high degree of variability between casts and between individual tubes from a single cast. We could not obtain a coefficient of determination (R^2) greater than 0.1 for an exponential, logarithmic, or linear regression of ^{134}Cs and $^{210}Pb_{ex}$ inventories, which confirms that the factors controlling inventories at the local scale vary for the two isotopes (Supplement S3).

Although we observed large tube to tube differences in the cesium activities, the grain size results for each of the 8 subcores were relatively similar in magnitude (Supplement S4). D50 values ranged from 19 to 41 μm, percent clay from 7.3 to 12, and percent fines from 66 to 85.

Although a study of the Irish Sea found elevated ^{137}Cs activities with increasing percentages of higher surface area particles (Poole et al., 1997), such as clays, we could not find any relationship (exponential, linear, or logarithmic) with an R^2 value of greater than 0.1 between the three grain size parameters and cesium activities or inventories at this single site (Supplement S5). $^{210}Pb_{ex}$ activities showed some relationship with percent clay in the replicate cores (R^2 values ranging from 0.34 to 0.36). While Kusakabe et al. (2013) posited that low bulk densities could indicate finer grain sizes and abundant organic matter content, we did not see evidence of this in the replicate cores. Although particle size characteristics do not appear to control local differences in radionuclide activities, where variations in average particle size and abundances of particle types (clays, etc) are relatively small, they may be important over larger regional scales where mineralogical differences are greater (See Sect. 3.5).

3.2 Zonal Divisions

Previous studies have delineated various coastal regions to estimate the total cesium delivery to the sediments near FDNPP. Kusakabe et al. (2013) used a boundary from approximately 35.5°N to 38.5°N, while Otosaka and Kato (2014) used incremental isobaths running from 35.67°N to 38.50°N to create 8 separate zones (0 to 1500 m). For consistency, we used 35.5°N to 38.5°N for our northernmost and southernmost zonal boundaries and isobaths for eastern and western divisions (Fig. 1 and Table 1). We divided the sediment reservoir into five zones based on inventories, grain size, and mixing rate estimates from our 20 sediment cores (See Sect. 3.3 to 3.7). The northern coastal zone (NCZ, n = 6) and southern coastal zone (SCZ, n = 3) are bound by the 150 m isobath to the east. The northern and southern boundaries of the NCZ and SCZ were shortened to 38.20°N and 36.25°N, respectively, after consideration of additional surface cores from MEXT (Kusakabe et al., 2013) (See Sec. 3.9). The mid-coastal zone (MCZ, n = 5) is bound by the 800 m isobath to the east, and the Japanese coast, NCZ, and SCZ to the west. The offshore zone (OZ, n = 4) is bound to the west and east by the 800 m and 4000 m isobaths, respectively. We included core 3 (4066 m) in the OZ because of its proximity to core 4 and an under representation of deeper cores in this zone. The remaining cores (n = 2) are located in the abyssal zone (AZ). All result and calculations in the following sections will be discussed relative to these zones.

3.3 Grain Size Analysis

Two cores from the OZ and all cores from the NCZ, SCZ, and MZ were analyzed by layer with a Beckman Coulter counter and the results were averaged by core (Table 1). The remaining 4 cores were visually assessed with a hand lens and assigned a general size class relative to the Udden-Wentworth Classification scheme. The NCZ cores contained the lowest percent clay (0.2 to 0.8%) and yielded the highest D50 values, ranging from 160 to greater than 690 μm. These cores were composed of relatively well-sorted sands and D50 standard deviations were generally less than 10% of the D50 value. The SCZ cores contained more poorly sorted grain assemblages and could be characterized as mostly silt-dominated with some fine sands. D50 values for these cores ranged from 33 to 80 μm, an order of magnitude lower than those observed in the NCZ, and the percent clay ranged from 5 to 9%, an order of magnitude higher than those in the NCZ. The MCZ cores were fairly similar in characteristics to the SCZ cores and ranged from 5 to 10% clay and in D50 from 40 to 110 μm. The two OZ cores were very fine-grained and had relatively similar D50 and percent clay values of approximately 18.5 μm and 12.5%, respectively.

The average values for D50, percent fines, and percent clay reflected wide variations in grain size from the coastal to offshore regions, although for a given core the changes in grain size between individual layers from top to bottom were generally small. We saw that as water depth increased to 5900 m, average grain sizes generally transitioned from coarser sands and granules (0.5 to 4 mm) to very fine silts and clays (<63 μm). This broad relationship did not always hold true in the near-shore, however, as the NCZ and SCZ cores differed in average grain size characteristics but not in water depth. Although a few cores showed D50 layer variations up to 220 μm over 2 cm increments, no observable pattern existed when these fluctuations were compared with changes in isotope activities. Conversely, many large layer to layer cesium fluctuations, like those seen in core 17, could not be explained by changes in grain size. Despite the likelihood that some or all of the cores might contain tsunami deposits, there was no grain size evidence of fining-upward sequences in these cores, sharp layer contacts with largely differing grain sizes, or definitive indicators that would allow us to separate potential tsunami layers from sections impacted by bio-irrigation, bioturbation, or local physical processes (Sakuna et al., 2012).

3.4 Cesium Activity Profiles

Average surface activities for the top 3 cm in the cores ranged from 2.1 ± 0.1 (core 2, C2) to 630 ± 30 (C20) Bq kg^{-1} dry for ^{137}Cs and from 0 (C2) to 550 ± 30 (C20) Bq kg^{-1} dry for ^{134}Cs (Supplement S6). The AZ cores contained no detectable ^{134}Cs. The average surface activities in the OZ ranged from 0 (C3) to 12 ± 1 (C6) Bq kg^{-1} dry for ^{134}Cs, while the MCZ activities ranged from 3 ± 0.5 (C7) to 57 ± 2 (C11) Bq kg^{-1} dry for ^{134}Cs. NCZ cores 15 through 19 had a similar range of average surface activities from 19 ± 1 (C16) to 50 ± 2 (C18) Bq kg^{-1} dry. While most surface ^{134}Cs activities in the NCZ were unexpectedly low, despite their proximity to the FDNPP, core 20, located within 3 km of the FDNPP, had the highest average surface activity overall. With the exception of this core, the cores in the SCZ had the greatest average surface activities of all zones, with ^{134}Cs values ranging from 170 ± 10 (C13) to 230 ± 10 (C14) Bq kg^{-1}.

Cesium profiles varied strongly in shape and penetration depth between zones (Fig. 2). Cores in the AZ and OZ had either fallout-only profiles with no ^{134}Cs and very low ^{137}Cs or rapidly decreasing ^{134}Cs and ^{137}Cs activities with depth. FDNPP-derived cesium penetration was limited to the top 3 cm in these zones. The MCZ cores generally showed similar exponentially decreasing cesium activities with depth with the exception of core 11, which showed a pronounced peak between 1 and 4 cm. Generally, the penetration depth of ^{134}Cs was deeper here than in the AZ and OZ cores. The SCZ cores maintained substantially higher cesium activities from 0 to 8 cm relative to most other cores and we observed both exponentially decreasing activities and vertical profiles below 8 cm. ^{134}Cs was found to a depth of 18 cm in core 12 and over the full length of cores 13 (19 cm) and 14 (16 cm) in the SCZ. While the NCZ cores had similar surface activities to those in the MCZ, most cores in this zone showed distinctive semi-vertical profiles from the surface to the coring depths. Core 17 was the only exception and the only core to exhibit activity large fluctuations with depth. Because we observed ^{134}Cs at all core bottoms and without decreasing trends in most of the NCZ cores, we could not estimate maximum penetration depths.

3.5 Cesium Inventories

Total ^{134}Cs and ^{137}Cs inventories ranged from 0 (C1) to 74,000 ± 2,000 (C20) Bq m^{-2} and 21 ± 1 (C3) to 73,000 ± 2,000 (C20) Bq m^{-2}, respectively (Table 1). Our inventory range for ^{137}Cs was almost four times larger than those reported in Kusakabe et al. (approximately 100 to 18,000 Bq m^{-2}; 2013) and Otosaka and Kato (approximately 100 to 19,100 Bq m^{-2}; 2014). This could be

attributed to both greater core lengths and larger total area sampled, including the 30 km zone around the FDNPP. Cesium inventories generally decreased with water depth. AZ and OZ inventories were less than 400 Bq m^{-2} for both isotopes and the MCZ contained only one core inventory above 1,000 Bq m^{-2}. Excluding core 20, we observed cesium inventories on the order of 1,500 to 7,000 Bq m^{-2} in the NCZ and 4,000 to 36,500 Bq m^{-2} in the SCZ. The cesium inventories for core 20 were double that of the next highest value and reflected a proximity to the FDNPP. Pre-accident cores from the broader western north Pacific have been reported to contain 10s to 1000s of Bq m^{-2} of ^{137}Cs (Moon et al., 2003; Lee et al., 2005). Assuming a weapons testing delivery of 2500 Bq m^{-2} for 30° to 40° N (Bowen et al., 1980) and 1-5% delivery to the sediments, we expect an average sediment inventory of ^{137}Cs less than 50 Bq m^{-2} prior to Fukushima. We observed inventories consistent with the presence of substantial weapons testing fallout in the AZ and OZ cores with inventory ratios for $^{134}Cs/^{137}Cs$ of 0 to 0.86. Larger inventories and $^{134}Cs/^{137}Cs$ ratios of ~1 in most of the MCZ, NCZ, and SCZ cores suggested negligible contributions from weapons testing ^{137}Cs, relative to the larger and more recent FDNPP source.

Since many prior studies have focused on the 0 to 3 cm surface layer, we also calculated the percentage of total inventory that lay below 3 cm within each of our cores (Table 1). Percentages generally increased with shallower water depths. We observed 75 ± 6% and 75 ± 5% for ^{134}Cs and 73 ± 7% and 75 ± 5% for ^{137}Cs (mean ± std. dev.) below 3 cm as a fraction of the total inventory in the NCZ and SCZ, respectively. In the MCZ, the percentage of total inventory below 3 cm was highly variable, ranging from 0 (C7 and C10) to 33% (C8) for ^{134}Cs and from 10 (C10) to 36% (C8) for ^{137}Cs. The average inventory below 3 cm in the MCZ cores attributed to Fukushima (^{134}Cs) was 15 ± 16%, which agreed closely with the Otosaka and Kato (2014) ^{134}Cs average of 19% from core locations within the MCZ. When we combined the two datasets for the MCZ (n = 15) the average inventory below 3 cm was 18 ± 16%. In the OZ we saw no ^{134}Cs below 3 cm in any of the cores and a range of 0 (C3) to 32% (C4) for ^{137}Cs. We did not observe any detectable amount of either isotope below 3 cm in the AZ.

The core inventories from this study reflect changes in three main factors: distance from the FDNPP, water depth, and grain size. Proximity impacted core 20, located within 3 km of the FDNPP (Fig. 3A). Figure 3A, shows a general decrease in cesium inventories with increasing distance from the FDNPP and water depth, despite that cesium inventories for cores 1 to 19 show

little to no statistical relationship to proximity or water depth (exponential regression R^2 values < 0.25). Grain size was a controlling factor in the near-shore NCZ and SCZ, where cores were sampled from similar water depth ranges and yet contained widely varying inventories (Table 1, Fig. 3A). Although no trend was observed in our replicate core tubes between grain size and cesium activities, the larger differences in grain size between the SCZ and NCZ (D50s from ~30 to 700 µm) did correspond to changes in total ^{134}Cs inventories. The NCZ and SCZ grain size trends mimic those observed in the Irish Sea, where an estimated 41 PBq of cesium released over 40 years has been preferentially incorporated into an area known as the Sellafield mud patch (Poole et al., 1997). In summary, proximity dominated within the 3 km zone of FDNPP, despite the high sand content of core 20 (D50 of 160 µm, percent sand ~94%), grain size was the most important difference between the NCZ and SCZ, and water depth (higher particle fluxes are generally observed over more productive coastal waters) may have contributed to cesium variability in locations such as the MCZ and OZ, where water column activities were relatively low.

3.6 $^{210}Pb_{ex}$ and $^{234}Th_{ex}$ Activities and Inventories

$^{210}Pb_{ex}$ surface activities (0 to 3 cm average) ranged from 12 ± 3 (C20) to 1,900 ± 100 (C1) Bq kg^{-1} and generally increased with water depth, as expected, due to the increased input from water column scavenging (Supplement S6, Figs. 1 and 2). $^{210}Pb_{ex}$ activities were lowest in the NCZ and highest in the AZ. Intra-zonal $^{210}Pb_{ex}$ activity ranges were smaller than for cesium. Similar to the vertical cesium activity profiles, $^{210}Pb_{ex}$ activities remained relatively constant with depth in the NCZ. In the other zones, activities generally decreased with core depth, but also exhibited a variety of profile shapes. Generally, the termination of $^{210}Pb_{ex}$, the depth where all ^{210}Pb is supported, was not attained within our sampling depths, with the exception of cores 3 and 6 (Fig. 2).

$^{210}Pb_{ex}$ inventories, ranging from 2,700 ± 200 (C18) to 28,000 ± 1,000 (C1) Bq m^{-2}, reflect changes in grain size, water depth and local processes, the factors that also impacted cesium inventories (Table 1, Fig. 1 and 3B). $^{210}Pb_{ex}$ inventories generally increased with water depth as expected from scavenging. The NCZ values were slightly lower than anticipated (average inventory of 4,000 ± 1000 Bq m^{-2}) based on our expected atmospheric inventory calculation of 6400 Bq m^{-2} and the SCZ values were more than twice as high as expected (average inventory

412 20,000 ± 10,000 Bq m^{-2}). The SCZ zone is therefore a deposition center, receiving additional
413 particles via horizontal transport. These trends are supported by the prevalence of sands in the
414 NCZ cores and higher percentages of fines in the SCZ cores, similar to that observed with
415 cesium inventories (He and Walling, 1996). An exponential regression of $^{210}Pb_{ex}$ inventories
416 versus percent clay in the NCZ and SCZ indicated a strong relationship (R^2>0.9) between grain
417 size and inventories. The MCZ, OZ, and AZ core inventories of $^{210}Pb_{ex}$ were generally one to
418 four times higher than atmospheric delivery. This finding is similar to along the shelf and slope
419 of the northeast U.S.A. (Buesseler et al., 1985/1986) and can be attributed to both scavenging
420 within the water column, which is higher with increasing water depth, and horizontal transport
421 and faster scavenging rates over boundary sediments in general. Evidence of boundary
422 scavenging of ^{210}Pb has been shown for the NW Pacific by Cochran et al. (1990) based upon an
423 analysis of deep sediment cores and the expected inventories from water column scavenging and
424 atmospheric sources.

425 Of the 17 cores that were analyzed rapidly enough to measure $^{234}Th_{ex}$, 15 contained
426 $^{234}Th_{ex}$ activities ranging from 17 ± 3 (C19) to 1300 ± 100 (C12) Bq kg^{-1} in the top 0 to 0.5 cm.
427 Surface (0 to 3 cm) $^{234}Th_{ex}$ inventories peaked at 2,400 ± 300 (C14) Bq m^{-2} in the SCZ. Most
428 cores showed classic exponential $^{234}Th_{ex}$ profile shapes with higher values at the surface that
429 dropped to near zero excess values within 1 to 3 cm. Although the lowest $^{234}Th_{ex}$ inventories
430 were found in the OZ and NCZ and the highest were generally located in the SCZ and MCZ,
431 intra-zonal variability was high and more often than not inventories did not decrease with
432 increasing depth.
433

434 **3.7 D_B Estimates**

435 Since all of the cores showed evidence of sediment mixing, we estimated local mixing rates
436 using $^{234}Th_{ex}$ and $^{210}Pb_{ex}$ activity profiles and a steady-state diffusive mixing model (Eqs. 2 and 5,
437 See Fig. 4 for example profile). Mixing rates in the MCZ, OZ, and AZ ranged from 0.7 (C9) to
438 9.6 (C10) cm^2 yr^{-1} for $^{234}Th_{ex}$-derived estimates and from 0.06 (C1) to 3.7 (C10) cm^2 yr^{-1} for
439 $^{210}Pb_{ex}$-derived estimates (Table 2). At a given location, $^{234}Th_{ex}$-derived estimates were
440 generally higher as they reflect processes occurring in the uppermost active sediment layers
441 (Aller and Cochran, 1976). Rates in the SCZ and NCZ suggested intense mixing, with full core
442 $^{210}Pb_{ex}$-derived estimates starting at 11 cm^2 yr^{-1} and the majority of rates being unquantifiable

443 due to the vertical $^{210}Pb_{ex}$ profiles. The wide range in rates was not unexpected with cores from
444 diverse sedimentary environments and water depths. While $^{234}Th_{ex}$-derived mixing rates were
445 not correlated with water depth (R^2<0.1) we observed an exponentially decreasing trend in
446 $^{210}Pb_{ex}$-derived mixing rates with water depth (R^2 = 0.96), as observed in other coastal regions
447 where biomass, species diversity, and bioturbation decrease with depth (Henderson et al., 1999;
448 Joydas and Damodaran, 2009).

449 Although $^{234}Th_{ex}$ was absent from some of the deepest AZ, OZ, and MCZ cores, we
450 succeeded in obtaining $^{210}Pb_{ex}$ and $^{234}Th_{ex}$ mixing rates for most cores located in these zones. In
451 general, the activity profiles exponentially decreased with depth (Figs. 2 and 4) and the AZ and
452 OZ $^{210}Pb_{ex}$-derived mixing rates agreed well with the observed historical rates from this region of
453 0.1 to 1 $cm^2\ yr^{-1}$ (Moon et al., 2003; Yang et al., 1985). Cores from the shallowest regions (NCZ
454 and SCZ) were the most difficult to fit with the simplified sediment mixing-only model (Eq. 5).
455 The SCZ cores generally contained 3 layers of mixing: a 1 to 3 cm moderately fast mixing zone
456 at the surface, a 5 to 10 cm rapid mixing layer with an almost vertical profile, and a deep mixing
457 zone with similar mixing rates as the surface layers. Equation (5) could not be used at all to
458 derive $^{210}Pb_{ex}$ mixing rates for any of the NCZ cores due to the almost vertical activity profiles
459 throughout. In these instances, the observed profile trends could have resulted from extremely
460 rapid mixing or from resuspension and deposition resulting from a tsunami or storm-related
461 event although we did not see evidence of individual storm deposits in the grain size analysis
462 (See Sect. 3.3).
463

464 **3.8 Cesium Modeling of Changes in Surface Activities**

465 To explore how quickly sediment mixing could potentially reduce surface (0 to 3 cm) cesium
466 activities over time we calculated the change in surface cesium activity, assuming a pulse-like
467 input (Eq. 6). The $^{234}Th_{ex}$-derived mixing rate was used for the depths specified in Table 2 and
468 the corresponding $^{210}Pb_{ex}$-derived mixing rate was used for the rest of the core. If no rate existed
469 for one of the isotopes, the mixing rate from the other was applied to all depths. The decay of
470 ^{137}Cs, although small over 5 to 10 years was subtracted from the profile activities after all other
471 calculations to show changes due to mixing only. In general, the measured cesium activity
472 profiles for the top 3 cm matched fairly well with the pulse model output for our sampling dates
473 using the local bioturbation rate. Below 3 cm, the model generally followed the AZ, OZ, and

MCZ measured cesium profiles (See Fig. 4 for example profile) and underestimated the NCZ and SCZ profiles.

The time until the surface (0 to 3 cm) activities decreased by 50% ranged from 0.4 (C14) to 26 (C1 and C3) years for the 20 cores (Table 2). The SCZ times ranged from 0.4 (C14) to 0.9 (C13) years and the MCZ times from 2 (C10) to 15 (C8) years. We could not model any of the cesium profiles in the NCZ using $^{210}Pb_{ex}$ mixing rates and the two with $^{234}Th_{ex}$ mixing rates yielded estimates from 12 (C16) to 14 (C15) years, which seemed unrealistically long when the considering the water depth and shape of the vertical profiles. The longest time period for decrease will occur in the slow-mixing OZ and AZ regions, whose 50% reduction time varied from 6 (C4) to 26 (C1 and C3) years.

3.9 Total Seafloor Cesium Inventory Calculations

We estimated that the marine sediments contained approximately 100 ± 50 TBq of ^{137}Cs for an area of 55,000 km^2 (Tables 3A and 3B). The final totals for each zone were calculated by finding the mean inventory of all cores within that zone and multiplying by the area of the zone. Zonal and final totals are reported with standard deviations for dataset (1), cores from this study only, in Table 3B. Inventory calculations should represent underestimates of actual reservoir totals because the profiles in the highest inventory zones, the NCZ and SCZ, still showed Fukushima ^{134}Cs in their deepest sample layers. We did not calculate an inventory value for the AZ, which is extensive, but should not significantly contribute to overall inventories due to low cesium activities. Furthermore, the cores from the greatest water depths, 1 and 2, did not contain Fukushima ^{134}Cs, although it has been detected in sediments as far offshore as the Japan Trench (water depth of >7000 m; Oguri et al., 2013).

To improve our inventory estimate, we added cores recovered in February 2012 by MEXT (Kusakabe et al., 2013) and from August to November 2011 reported in Otosaka and Kato (2014) (OTKA). These provided an additional 50 locations, referred to as datasets (3) and (2), respectively. The inventories of the shorter sediment cores were increased using the average percent ^{134}Cs inventory below 3 and 10 cm determined for each zone when applicable (See Sect. 3.5). Cesium activity and inventory values from the MEXT and OTKA datasets were not changed if the depth sampled was sufficient to capture the full extent of cesium penetration. The

additional locations did not impact the sediment inventory estimate, now 100 ± 40 TBq, and did not substantially change the distribution of cesium between zones (Tables 3A and 3B).

In a final effort to further improve our inventory estimates, we utilized all earlier sampling dates from the 30 MEXT locations in Fig. 5 and calculated a total sediment reservoir estimate of 130 ± 60 TBq (n = 199, Table 3B). These locations were sampled at approximately monthly intervals starting June 2011 and are referred to as dataset (4). As we have observed, the range in local variability can be almost as high as that on the zonal or regional scale (Kusakabe et al., 2013; Thornton et al., 2013) so additional sampling at one site should not bias the zonal averages towards these repeated locations. However, because of the much earlier sampling dates for the MEXT cores relative to our last date in September 2013 and the 3 cm sampling length, we considered the sensitivity of our inventory estimate to mixing, which could transport cesium to deeper layers between sampling events. Using Eq. (6) and the estimates of mixing rates, we determine the average percent of cesium below 3 cm for each zone in June 2011 and used these smaller percentages instead of those in Section 3.5 to adjust the MEXT data. After this adjustment, the total inventory estimate decreased slightly to 100 ± 60 TBq.

The three approximation methods all resulted in similar total ^{137}Cs sediment inventories, ranging from 100 to 130 TBq (Tables 3A and 3B). The OZ comprised more than half the entire area but consistently totaled only 4 to 6% of the ^{137}Cs sediment inventory. The MCZ represents 30% of regional surface area and contained between 15 and 18 percent of the total ^{137}Cs. The NCZ was split into two subzones to account for the extremely high inventory observed within the 3 km radius of the FDNPP. Based on Thornton et al.'s continuous tow data, the area immediately around the nuclear facility (~3 km) showed the largest number of high ^{137}Cs Bq kg^{-1} anomalies relative to adjacent sediments (Thornton et al., 2013). Core 20 confirmed that this region was distinctly higher in activity and warranted its own subzone, so as not to skew the NCZ inventory average. The 3 km subzone adjacent to the FDNPP accounted for approximately 1% of the total inventory. Although, this inventory could change with the addition of new and deeper cores, because the 3 km subzone only comprises 0.03% of the total area, even assuming a mixed layer depth of 50 cm (cesium penetration to 50 cm; Walbran, 1996) would not change the total regional inventory more than a few TBq. The NCZ and the SCZ, on the other hand, contributed the most cesium by far (over 70%), yet composed only 9% and 6% of the total area, respectively (Tables 3A and 3B).

Figures 5 and 6 show the spatial distribution of cesium inventories for all zones surrounding the FDNPP and illustrate both the high intra-zonal variability and the overall decrease of inventories with depth. Included are cores from this study (n = 18), from the February 2012 MEXT sampling dates (n = 30; Kusakabe, 2013), and from all OTKA dates (n = 20; Otosaka and Kato, 2014), the latter two containing adjusted cesium inventories when applicable (See Sect. 3.5). Best fit exponential regressions of these inventories versus water depth are shown in Fig. 6. As observed with the cores from this study, the complied inventories from 0 to 150 m in the NCZ and SCZ did not reflect a significant relationship with water depth (R^2 <0.01), which we suggest reflects the importance of grain size distribution in these zones (Fig. 3A).

4 Conclusions

Our ^{137}Cs sediment inventory estimates of 100 to 130 TBq for 55,000 km^3 (0 to 4000 m water depth off Japan) represent the most comprehensive attempt to date for quantifying FDNPP cesium incorporation into marine sediments. The coastal sediments contain the majority of the total TBq delivered, with inventories ranging from 100 to 125 TBq for 24,100 km^2 (0 to 800 m water depth). With expanded spatial coverage inside the 30 km radius of the FDNPP and improved vertical resolution in the NCZ and SCZ, our coastal inventory estimates fall between Kusakabe et al.'s (2013) 38 TBq and Otosaka and Kato's (2014) 200 TBq. Kusakabe et al. (2013) had calculated only surface inventories for the upper 3 cm for a similar area, thus providing a lower limit for total coastal inventories. Otosaka and Kato's (2014) estimate of 200 TBq is higher because it was calculated using exponential water depth versus cesium inventory relationships that were derived without any NCZ cores, which effectively applied the relatively elevated SCZ core inventories to the entire NCZ and SCZ (Fig. 5).

Our zonal analysis of cesium inventories, in conjunction with $^{210}Pb_{ex}$ and grain size analyses, has provided an assessment of the total cesium inventory that will inform future studies. We have identified key areas where more cores may improve inventory estimates. First, additional sampling is needed to supplement sparse coverage in two regions: north of the FDNPP along the coast, from 37.70°N to 38.20°N in the MCZ, and in locations deeper than 2000 m in the OZ. With the large observed spatial variability from scales of 1 m^2 (between multi-corer tubes) to 10,000 m^2 (among zones) greater numbers of cores are essential to give better constrain our estimates at present. Second, while most MCZ and OZ cores are long enough to capture

566 complete cesium inventories, in the NCZ and SCZ cesium had penetrated deeper than 18 to 20
567 cm. More extensive and deeper coring in both zones is needed to determine ultimate penetration
568 depths and full inventories.

569 Both the relative inventories of cesium in the coastal environment and estimated zonal
570 'recovery' timescales have implications for bottom-dwelling biota and those that may consume
571 demersal species. If we assume a total ^{137}Cs release to the ocean of approximately 15 to 30 PBq
572 from the Fukushima accident (Buesseler, 2014), our calculated sedimentary inventories comprise
573 less than 1.0% of the total release in 2011. However, cesium concentrations in the water are
574 decreasing and only 15 TBq remain in coastal waters (Buesseler, 2014). Therefore, the sediment
575 reservoir currently represents approximately 86 to 90% of the total ^{137}Cs inventory (water and
576 sediment) off the coast of Japan. Rapid mixing in some locations may decrease biological access
577 to these high activity sediments by transporting cesium isotopes deeper and therefore decreasing
578 the overall activity of the more easily resuspended surface layers. While the MCZ and OZ
579 require more time to reduce surface activities by 50%, they do not pose as much of an
580 environmental hazard because of their relatively low initial activities. The areas of greatest
581 concern are the coastal zones shallower than 150 m water depth. Additional biological studies
582 should take note of these zonal hotspots as cesium levels may remain elevated here much longer
583 despite faster observed mixing rates.

584 In addition to bioturbation, other processes impacting cesium distributions in the coastal
585 ocean require further study. Yamashiki et al. (2014) found that suspended particle loads in the
586 Abukuma River Basin near Fukushima delivered over 5 TBq of cesium to the NCZ in a 10
587 month period. A typhoon that occurred during this time contributed more than half of this
588 inventory over only 8 days. While 5 TBq would account for only 4 to 5% of the total sediment
589 reservoir, depending on where and how the particles are transported this contribution could
590 create local hot spots. Chemical remobilization rates of cesium from sediment pore waters have
591 not been published for this area of Japan, but are likely less than 0.1 TBq per month for cesium,
592 based on previous studies of the Irish Sea (Mitchell et al.,1999), and could decrease the total
593 coastal inventory. Even though these source and loss terms are relatively small compared to the
594 total cesium inventory of the sediments, only long term monitoring within the study region will
595 indicate whether decay alone or other factors are controlling cesium activities and distributions
596 over the next decade.

5 Acknowledgements

The authors would like to thank the captain, crew, and scientists aboard the R/V Tunsei Maru, R/V Mirai, R/V Umitaka Maru, and the R/V Daisan Kaiyo Maru. In particular, our samples were made possible by collaborations in the field with Jota Kanda, Jun Nishikawa, Makio Honda, and Shigeyoshi Otosaka. Field and laboratory assistance was provided by Crystal Brier, Stephanie Madsen, Chris Griner, and Steven Pike. The authors would also like to acknowledge the support of the Gordon and Betty Moore Foundation, Deerbrook Charitable Trust, Woods Hole Oceanographic Institution, and Massachusetts Institute of Technology.

References:

Aller, R.C. and Cochran, J.K., $^{234}Th/^{238}U$ disequilibrium in near-shore sediment: particle reworking and diagenetic time scales. Earth Planet. Sc. Lett., 29, 37-60, 1976.

Anderson, R.F., Bopp, R.F., Buesseler, K.O., and Biscaye, P.E., Mixing of particles and organic constituents in sediments from the continental shelf and slope off Cape Cod: SEEP-I results. Cont. Shelf. Res., 8(5-7), 925-946, 1988.

Aoyama, M., Tsumune, D. and Hamajima, Y., Budgets and temporal change of radiocaesium distribution released from Fukushima NPP accidents in the North Pacific Ocean. Ocean Sciences Meeting, Salt Lake City, Utah, Feb 21, Session 88, 2012.

Bowen, V.T., Noshkin, V.E., Livingston, H.D., and Volchok, H.L., Fallout radionuclides in the Pacific Ocean: Vertical and horiztonal distributions, largely from GEOSECS stations. Earth Planet. Sc. Lett., 49, 411-434, 1980.

Buesseler, K.O., Fishing for answers off Fukushima. Science, 338, 480-482, 2012.

Buesseler, K.O., Fukushima and ocean radioactivity. Oceanography, 27(1), 1-13, 2014.

Buesseler, K.O., Livingston, H., and Sholkovitz, E., 239,240Pu and excess 210Pb inventories alon gthe shelf and slope of the northeast U.S.A. Earth Planet. Sc. Lett., 76, 10-22, 1985/1986.

Buesseler, K.O., Aoyama, M. and Fukasawa, M., Impacts of the Fukushima Nuclear Power Plants on marine radioactivity. Environ. Sci. Technol., 45, 9931-9935, 2011.

Buesseler, K.O., Jayne, S.R., Fisher, N.S., Rypina, I.I., Baumann, H., Baumann, Z., Breier, C.F., Douglass, E.M., George, J., Macdonald, A.M., Miyamoto, H., Nishikawa, J., Pike, S.M., Yoshida, S., Fukushima-derived radionuclides in the ocean and biota off Japan. P. Natl. Acad. Sci. U.S.A., 109(16), 5984-5988, 2012.

Charette, M.A., Breier, C.F., Henderson, P.B., Pike, S.M., Rypina, I.I., Jayne, S.R., and Buesseler, K.O., Radium-based estimates of cesium isotope transport and total direct ocean discharges from the Fukushima Nuclear Power Plant accident. Biogeosciences, 10, 2159-2167, 2013.

Chino, M., Nakayama, H., Nagai, H., Terada, H., Katada, G., and Yamazawa, H., Preliminary estimation of release amounts of ^{131}I and ^{137}Cs accidentally discharged from the Fukushima Daiichi Nuclear Power Plant into the atmosphere. J. Nucl. Sci. Technol., 48(7), 1129-1134, 2011.

638 Cochran, J.K., Particle mixing rates in the sediments of the eastern equatorial Pacific: Evidence
639 from ^{210}Pb, ^{239,240}Pu and ^{137}Cs distributions at MANOP sites. Geochim. Cosmochim. Ac.,
640 49, 1195-1210, 1985.
641 Cochran, J.K., McKibbin-Vaughan, T., Dornblaser, M.M., Hirschberg, D., Livingston, H.D., and
642 Buesseler, K.O., ^{210}Pb scavenging in the North Atlantic and North Pacific Oceans. Earth
643 Planet. Sc. Lett., 97, 332-352, 1990.
644 Currie, L.A., Limits for qualitative detection and quantitative determination. Anal. Chem., 40(3),
645 586-593, 1968.
646 He, Q. and Walling, D.E., Interpreting particle size effects in the adsorption of ^{137}Cs and
647 unsupported ^{210}Pb by mineral soils and sediments. J. Environ. Radioactiv., 30, 117-137,
648 1996.
649 Henderson, G.M., Lindsay, F.N., and Slowey, N.C., Variation in bioturbation with water depth
650 on marine slopes: a study on the Little Bahamas Bank. Mar. Geol., 160, 105-118, 1999.
651 Honda, M.C., Kawakami, H., Watanabe, S., and Saino, T., Concentration and vertical flux of
652 Fukushima-derived radiocesium in sinking particles from two sites in the Northwestern
653 Pacific Oean. Biogeosciences, 10, 3525-3534, 2013.
654 Joydas, T.V. and Damodaran, R., Infaunal macrobenthos along the shelf waters of the west coast
655 of India, Arabian Sea. Indian J. Mar. Sci., 38(2), 191-204, 2009.
656 Kanda, J., Continuing ^{137}Cs release to the sea from the Fukushima Dai-ichi Nuclear Power Plant
657 through 2012. Biogeosciences, 10, 6107-6113, 2013.
658 Kusakabe, M., Oikawa, S., Takata, H. and Misonoo, J., Spatiotemporal distributions of
659 Fukushima-derived radionuclides in nearby marine surface sediments. Biogeosciences,
660 10, 5019-5030, 2013.
661 Lee, S.H., Povinec, P.P., Wyse, E., Pham, M.K., Hong, G.H., Chung, C.S., Kim, S.H., and Lee,
662 H.J., Distribution and inventories of 90Sr, 137Cs, 241Am and Pu isotopes in sediments of
663 the Northwest Pacific Ocean. Mar. Geol., 216(4), 249-263, 2005.
664 Mitchell, P.I., Condren, O.M., Vintró, L.L., and McMahon, C.A., Trends in plutonium,
665 americium and radiocaesium accumulation and long-term bioavailability in the western
666 Irish Sea mud basin. J. Environ. Radioactiv., 44, 223-251, 1999.
667 Moon, D., Hong, G., Kim, Y., Baskaran, M., Chung, C.S., Kim, S.H., Lee,H., Lee, S., and
668 Povine, P.P., Accumulation of anthropogenic and natural radionuclides in bottom
669 sediments of the Northwest Pacific Ocean. Deep-Sea Res. Pt. II, 50, 2649-2673, 2003.
670 Nozaki, Y. and Tsunogai, S., ^{226}Ra, ^{210}Pb and ^{210}Po disequilibria in the Western North Pacific.
671 Earth Planet. Sc. Lett., 32, 313-321, 1976.
672 Nuclear Regulation Authority of Japan (NRA), Readings of sea area monitoring in marine soil,
673 http://radioactivity.nsr.go.jp/en/list/247/list-1.html. Feb 10 2014 (2014a).
674 Nuclear Regulation Authority of Japan (NRA), Readings of sea area monitoring in sea area by
675 MEXT, http://radioactivity.nsr.go.jp/en/list/260/list-1.html. Feb 10 2014 (2014b).
676 Oguri, K., Kawamura, K., Sakaguchi, A., Toyofuku, T. Kasaya, T., Murayama, M., Fujikura, K.,
677 Glud, R.N., Kitazato, H., Hadal disturbance in the Japan Trench induced by the 2011
678 Tohoku-Oki earthquake. Scientific Reports, 3(1915), doi: 10.1038/srep01915, 2013.
679 Otosaka, S. and Kato, Y., Radiocesium derived from the Fukushima Daiichi Nuclear Power Plant
680 accident in seabed sediments: Initial deposition and inventories. Accepted: Environ. Sci.
681 Processes and Impacts: pp. 28, 2014.

682 Otosaka, S. and Kobayashi, T., Sedimentation and remobilization of radiocesium in the coastal
683 area of Ibaraki, 70 km south of the Fukushima Dai-ichi Nuclear Power Plant. Environ.
684 Monit. Assess, 185, 5419-5433, 2013.
685 Poole, A.J., Denoon, D.C. and Woodhead, D.S., The distribution and inventory of ^{137}Cs in sub-
686 tidal sediments of the Irish Sea. In: P. Germain, J.C. Guary, P. Gueguenait and H.
687 Metivier (Editors), Radioprotection: Radionuclides in the Ocean Les Editions de
688 Physique, France, 32, pp. 422. 1997.
689 Povinec, P.P., Aoyama, M., Biddulph, D., Breier, R., Buesseler, K., Chang, C.C., Golser, R.,
690 Hou, X.L., Jeskovsky, M., Jull, A.J.T., Kaizer, J., Nakano, M., Nies, H., Palcsu, L., Papp,
691 L., Pham, M.K., Steier, P., and Zhang, L.Y., Cesium, iodine, and tritium in NW Pacific
692 waters – a comparison of the Fukushima impact with global fallout. Biogeosciences, 10,
693 5481-5496, 2013.
694 Sakuna, D., Szczucinski, W., Feldens, P., Schwarzer, K., and Khokiattiwong, S., Sedimentary
695 deposits left by the 2004 Indian Ocean tsunami on the inner continental shelf offshore of
696 Khao Lak, Andaman Sea (Thailand). Earth Planets Space, 64, 931-943, 2012.
697 Stohl, A., Seibert, P., Wotawa, G., Arnold, D., Burkhart, J.F., Eckhardt, S., Tapia, C., Vargas, A.,
698 and Yasunari, T.J., Xenon-133 and caesium-137 releases into the atmosphere from the
699 Fukushima Dai-ichi nuclear power plant: determination of the source term, atmospheric
700 dispersion, and deposition. Atmos. Chem. Phys., 11, 28319-28394, 2011.
701 Tateda, Y., Tsumune, D. and Tsubono, T., Simulation of radioactive cesium transfer in the
702 southern Fukushima coastal biota using a dynamic food chain transfer model. J. Environ.
703 Radioactiv., 124, 1-12, 2013.
704 Tokyo Electric Power Company (TEPCO), Measures for Water Leakage,
705 http://www.tepco.co.jp/en/nu/fukushima-np/water/index-e.html. Feb 10 2014.
706 Thornton, B., Ohnishi, S., Ura, T., Odano, N., Sasaki, S., Fujita, T., Watanabe, T., Nakata, K.,
707 Ono, T., and Ambe, D., Distribution of local ^{137}Cs anomalies on the seafloor near the
708 Fukushima Dai-ichi Nuclear Power Plant. Mar. Pollut. Bull., 74, 344-350, 2013.
709 Tsunogai, S. and Harada, K., ^{226}Ra and ^{210}Pb in the western North Pacific. In: E.D. Goldberg, Y.
710 Horibe and K. Saruhashi (Editors), Isotope Marine Chemistry. Uchida Rokakuho
711 Publishing Company, Tokyo, pp. 165-191, 1980.
712 Ueno, T., Nagao, S. and Yamazawa, H., Atmospheric deposition of ^{7}Be, ^{40}K, ^{137}Cs and ^{210}Pb
713 during 1993-2001 at Tokai-mura, Japan. J. Radioanal. Nucl. Ch., 255(2), 335-339, 2003.
714 Walbran, P.D., ^{210}Pb and ^{14}C as Indicators of Callianassid Bioturbation in Coral Reef Sediment.
715 J. Sediment Res. A, 66(1), 259-264, 1996.
716 Yamamoto, M., Sakaguchi, A., Sasaki, K., Hirose, K., Igarashi, Y., and Kim, C.K., Seasonal and
717 spatial variation of atmospheric ^{210}Pb and ^{7}Be deposition: features of the Japan Sea side
718 of Japan. J. Environ. Radioactiv., 86, 110-131, 2006.
719 Yamashiki, Y., Onda, Y., Smith, H.G., Blake, W.H., Wakahara, T., Igarashi, Y., Matsuura, Y.,
720 and Yoshimura, K., Initial flux of sediment-associated radiocesium to the ocean from the
721 largest river impacted by Fukushima Daiichi Nuclear Power Plant. Scientific Reports,
722 4(3714), doi: 10.1038/srep03714, 2014.
723 Yang, H.-S., Nozaki, Y., Sakai, H., Nagaya, Y. and Nakamura, K., Natural and man-made
724 radionuclide distributions in Northwest Pacific deep-sea sediments: rates of
725 sedimentation, bioturbation and ^{226}Ra migration. Geochem. J., 20, 29-40, 1985.
726
727

Table and Figure Captions:

Table 1 Grain Size Results and Isotope Inventories For Sediment Cores By Zone. A general size was assigned to cores 1, 2, 3, and 5 after visual inspection, as grain size analysis was not possible for these cores. All other cores are described according to the Udden-Wentworth scale with sediment classifications, C (clay), M (silt), and S (sand), and size qualifiers vf (very fine), f (fine), m (medium), c (coarse), and vc (very coarse). The uncertainty on all inventory values represents the propagation of the counting uncertainty for each section (minimum 7%) as discussed in Section 2.3. D50, % Clay, and % Silt and Clay represent the average value for all layers within a given core and are reported with standard deviations.

* Grain size results for cores 15 and 16 represent the fraction of sediment passed through a 1 mm sieve, 68% of the total sample mass for C15 and 89% for C16. Total D50 for these samples would be higher than the reported values and the percent clay and percent silt plus clay would be lower. The extra mass cannot be accounted for in the table values because the grain size analyzer measures by counts.

ND Not detectable

-- Not analyzed

[1] Decay-corrected to FDNPP discharge maximum

Table 2 Mixing Rates and Model Results for Sediment Cores.

NP Not possible because no $^{234}Th_{ex}$ present or the $^{234}Th_{ex}$ or $^{210}Pb_{ex}$ profiles could not be modeled by the simplified sediment mixing-only model (Eqs. 2 and 5).

[1] Due to the limited number of surface $^{234}Th_{ex}$ points, the uncertainties reported represent the higher of the standard uncertainty of the model fit for variable D_B or 25% of D_B.

[2] Values represent the time in years since the Fukushima maximum for surface concentrations (0-3 cm) to decrease by 50% via mixing (modeled). The uncertainties reflect the mixing rate(s) used in the model.

Table 3A Zonal Statistics Used for Inventory Estimates. Cores from group (1) are from this study only. Samples in group (2) were taken from Otasaka and Kato (2014; OTKA). Group (3) includes MEXT cores from February 2012 only and group (4) contains

MEXT cores from (3) plus additional cores from the end of June 2011 through February 2012 (Kusakabe et al., 2013).

Table 3B Total ^{137}Cs Inventory Results by Zone and Datasets Used
Estimates of total marine sediment ^{137}Cs inventories were found for this study only (n = 18) and by including datasets from Otasaka and Kato (2014) and Kusakabe et al. (2013) that were adjusted by zone based on calculated average percent inventories observed below 3 to 10 cm. See Table 3A for group numbers.

Fig. 1 Core Locations with $^{210}Pb_{ex}$ Inventories. Larger map: contains core locations 3 to 20 and the northern coastal (NCZ), southern coastal (SCZ), mid-coastal (MCZ), offshore (OZ), and abyssal (AZ) zones. Lower right: shows core locations 1 and 2. Some of the reported values may underestimate total inventories at the locations where $^{210}Pb_{ex}$ continues to the core bottom (Fig. 2).

Fig. 2 Sediment Activity Profiles in Bq kg^{-1} for ^{134}Cs, ^{137}Cs, $^{210}Pb_{ex}$, and $^{234}Th_{ex.}$

Fig. 3 ^{134}Cs and $^{210}Pb_{ex}$ Inventories Relative to Water Depth and D50. Grain size distribution is shown for 16 of the 20 cores, including all of the NCZ, SCZ, and MCZ cores. Isotope inventories for ^{134}Cs (A) and $^{210}Pb_{ex}$ (B) show general depth trends with prominent grain size effects in the NCZ and SCZ.

Fig. 4 Example model best fit regressions for $^{210}Pb_{ex}$, $^{234}Th_{ex}$, and ^{137}Cs. for core 9. Mixing rates derived from the $^{210}Pb_{ex}$, $^{234}Th_{ex}$ profiles in the left panel were used in the cesium pulse model for the right panel. In general, the model similarly fit the profiles from the MCZ, OZ, and AZ. Model fits for the SCZ and NCZ were less successful due to almost vertical profiles for some cores.

Fig. 5 A compilation of sediment ^{137}Cs inventories from the coastal region around Japan, Japan Fukushima. Core inventories from this study are shown as measured from May 2012 to September 2013. MEXT cores from February 2012 (Kusakabe et al., 2013) and OTKA samples from August through November of 2011 (Otosaka and Kato, 2014) were adjusted as necessary by zone to include estimated inventories deeper than 3 cm and 10 cm, respectively (Section 3.5).

Fig. 6 Spatial Variations in ^{137}Cs Sediment Inventories With Water Depth. The measured and adjusted inventories from Fig. 5 are plotted against water depth. The upper figure shows the exponential regression for core inventories from 0 to 150 meters, excluding

789 core 20. The lower figure shows all inventories and the regression for cores located
790 from 150 to 1500 m.

Zone	No.	Water Depth (m)	D50 (µm)	% Clay (<4 um)	% Silt and Clay (<63.4 um)	Udden-Wentworth Classification	$^{210}Pb_{ex}$ (Bq m^{-2})	$^{234}Th_{ex}$ (Bq m^{-2})	^{134}Cs (Bq m^{-2})[1]	^{137}Cs (Bq m^{-2})[1]	% ^{134}Cs Inventory Below 3 cm	% ^{137}Cs Inventory Below 3 cm
Abyssal	1	5900	--	--	--	M	28,000 ± 1,000	--	ND	84 ± 3	ND	0
	2	5156	--	--	--	M	19,500 ± 700	--	ND	26 ± 1	ND	0
Offshore	3	4066	--	--	--	M	4,800 ± 200	50 ± 30	ND	21 ± 1	ND	0
	4	3259	18 ± 2	12 ± 2	87 ± 3	C to vfS	22,500 ± 600	320 ± 60	32 ± 5	73 ± 4	0	32 ± 3
	5	1300	--	--	--	M	15,400 ± 500	--	190 ± 10	220 ± 10	0	13 ± 1
	6	1260	19 ± 7	13 ± 2	83 ± 9	C to fS	16,800 ± 500	1,700 ± 100	280 ± 20	370 ± 10	0	3 ± 0
Mid-Coastal	7	546	40 ± 20	10 ± 2	70 ± 10	vfM to fS	7,900 ± 200	1,100 ± 100	55 ± 8	97 ± 4	0	29 ± 2
	8	497	50 ± 10	6.8 ± 0.7	62 ± 7	vfM to fS	16,100 ± 400	2,300 ± 100	870 ± 20	850 ± 20	33 ± 2	36 ± 2
	9	321	40 ± 10	7 ± 1	65 ± 7	vfM to fS	13,400 ± 300	800 ± 100	540 ± 30	540 ± 20	13 ± 1	21 ± 1
	10	309	100 ± 30	5 ± 1	40 ± 10	fM to mS	14,600 ± 400	1,000 ± 100	840 ± 30	840 ± 20	0	10 ± 1
	11	205	110 ± 90	7 ± 3	50 ± 20	vfM to mS	12,200 ± 400	1,500 ± 100	3,200 ± 100	2,900 ± 100	30 ± 1	32 ± 1
Southern Coastal	12	125	33 ± 9	9 ± 2	74 ± 7	vfM to fS	19,200 ± 400	1,500 ± 100	4,400 ± 100	3,800 ± 100	73 ± 4	72 ± 3
	13	125	40 ± 10	9 ± 2	68 ± 9	vfM to fS	19,700 ± 400	810 ± 80	13,700 ± 300	12,600 ± 300	69 ± 3	67 ± 3
	14	65	80 ± 20	5 ± 1	50 ± 10	vfM to fS	17,400 ± 400	2,400 ± 300	36,500 ± 800	30,300 ± 600	82 ± 3	81 ± 3
Northern Coastal	15	120	690* ± 60	0.3* ± 0.1	1.8* ± 0.8	mS to vcS	3,800 ± 200	200 ± 100	1,800 ± 100	1,650 ± 40	69 ± 5	69 ± 3
	16	60	540* ± 60	0.2* ± 0.1	1.1* ± 0.5	mS to vcS	4,600 ± 200	310 ± 40	2,900 ± 100	2,900 ± 100	77 ± 3	79 ± 3
	17	35	350 ± 10	0.6 ± 0.5	4 ± 4	fS to cS	6,600 ± 200	600 ± 100	6,800 ± 100	5,800 ± 100	83 ± 4	82 ± 3
	18	35	270 ± 7	0.2 ± 0.02	0.9 ± 0.2	fS to cS	2,700 ± 200	ND	6,700 ± 100	6,500 ± 100	76 ± 3	76 ± 3
	19	23	550 ± 40	0.2 ± 0.1	1.1 ± 0.6	mS to cS	3,300 ± 200	650 ± 80	5,700 ± 100	5,400 ± 100	75 ± 4	76 ± 4
	20	14	160 ± 10	0.8 ± 0.3	6 ± 2	vfS to mS	3,600 ± 200	ND	74,000 ± 2,000	73,000 ± 2,000	73 ± 5	69 ± 4

Black and Buesseler, Table 1

Zone	No.	$^{234}Th_{ex}$ - Derived D_B (cm^2 yr^{-1})[1]	Depths Used (cm)	$^{210}Pb_{ex}$ - Derived D_B (cm^2 yr^{-1})	Depths Used (cm)	Estimated Years Until 50% Decrease in Surface Cesium[2]
Abyssal	1	NP		0.06 ± 0.02	1.5-5	26 ± 2
	2	NP		0.6 ± 0.2	1.5-9	10 ± 2
Offshore	3	NP		0.07 ± 0.02	0.5-3	26 ± 2
	4	0.8 ± 0.2	0-2	NP		6 ± 2
	5	NP		0.5 ± 0.1	1.5-9	11 ± 2
	6	5.5 ± 4	0-1.5	0.09 ± 0.02	2-8	24 ± 1
Mid-Coastal	7	0.9 ± 0.7	0-3	0.8 ± 0.2	2-8	5 ± 2
	8	2.4 ± 0.6	0-2	0.3 ± 0.1	1.5-5	15 ± 1
	9	0.7 ± 0.2	0-2	0.8 ± 0.1	2-8	8 ± 1
	10	9.6 ± 3	0-2	3.7 ± 0.4	3-8	2 ± 1
	11	1.6 ± 0.4	0-1.5	0.6 ± 0.1	1.5-10	10 ± 1
Southern Coastal	12	2.7 ± 0.7	0-1.5	12 ± 2	1.5-20	0.8 ± 0.2
	13	NP		11 ± 2	0-19	0.9 ± 0.2
	14	2.5 ± 0.6	0-2	22 ± 6	2-16	0.4 ± 0.2
Northern Coastal	15	0.3 ± 0.1	0-2	NP		14 ± 2
	16	0.4 ± 0.1	0-2	NP		12 ± 4
	17	NP		NP		NP
	18	NP		NP		NP
	19	NP		NP		NP
	20	NP		NP		NP

Black and Buesseler, Table 2

	Zone	Depth Ranges (m)	Area (km^2)	% of Area	No. of Sample Points (1) This Study	(2) OTKA	(3) MEXT	(4) MEXT
	OZ	800 - 4000	30,832	56%	4	3	0	0
	MCZ	150 - 800	16,087	29%	5	10	17	77
	SCZ	0 - 150	3,309	6%	3	7	7	43
NCZ	Greater Area	0 - 150	4,731	9%	5	0	6	41
NCZ	3 km radius	0 - 150	14	0.03%	1	0	0	0
	Total	0 - 4000	54,973 km^2		18	20	30	161

Black and Buesseler, Table 3A

	Zone	This Study (1) Mean ^{137}Cs (Bq m^{-2})	This Study (1) Total ^{137}Cs TBq	This Study (1) % of Total TBq	(1) & (2) & (3) Mean ^{137}Cs (Bq m^{-2})	(1) & (2) & (3) Total ^{137}Cs TBq	(1) & (2) & (3) % of Total TBq	(1) & (2) & (4) Mean ^{137}Cs (Bq m^{-2})	(1) & (2) & (4) Total ^{137}Cs TBq	(1) & (2) & (4) % of Total TBq
	OZ	170 ± 160	5 ± 5	5.5%	160 ± 120	5 ± 4	4.8%	160 ± 120	5 ± 4	3.9%
	MCZ	1,000 ± 1,100	17 ± 17	17.6%	1,200 ± 1,000	19 ± 16	18.3%	1,200 ± 1,000	19 ± 16	14.8%
	SCZ	16,000 ± 13,000	52 ± 45	54.0%	13,000 ± 6,800	44 ± 22	42.3%	13,000 ± 8,700	42 ± 29	33%
NCZ	Greater Area	4,500 ± 2,100	21 ± 10	21.8%	7,300 ± 5,100	35 ± 24	33.6%	13,000 ± 11,000	61 ± 52	47.5%
NCZ	3 km radius	73,000	1	1.1%	73,000	1	1.0%	73,000	1	0.8%
	Total	100 ± 50 TBq			100 ± 40 TBq			130 ± 60 TBq		

Black and Buesseler, Table 3B

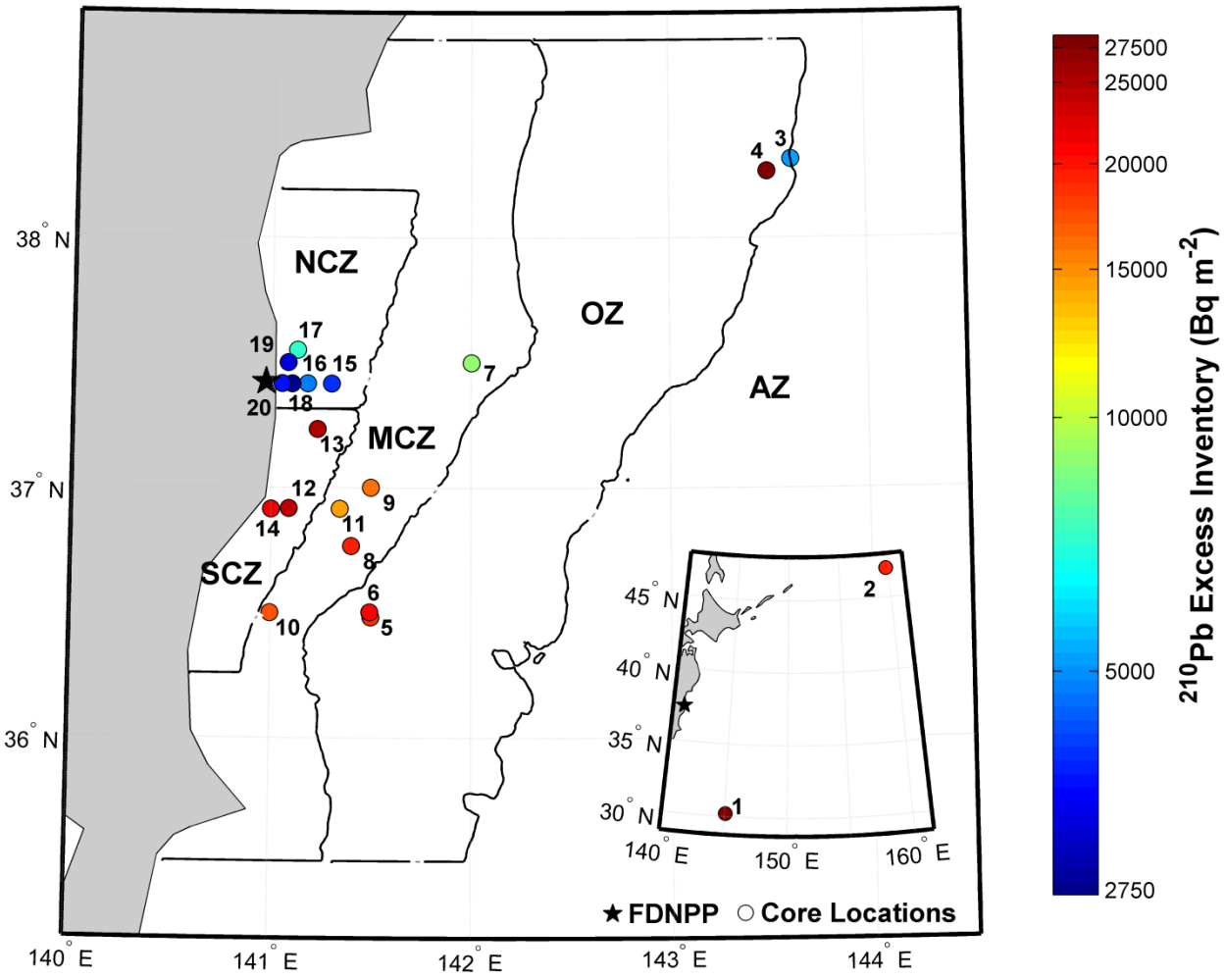

Black and Buesseler, Fig. 1

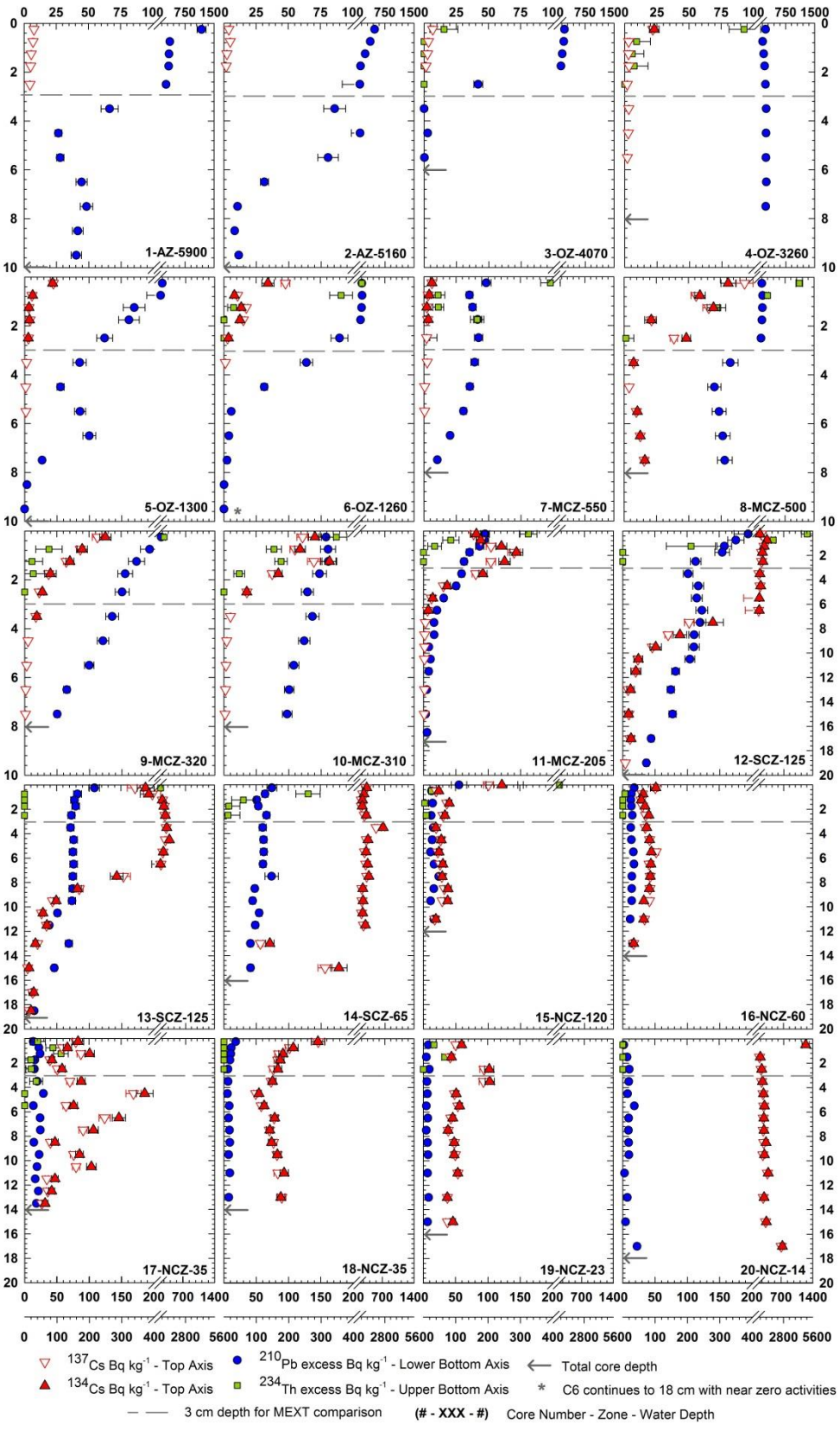

Black and Buesseler, Fig. 2

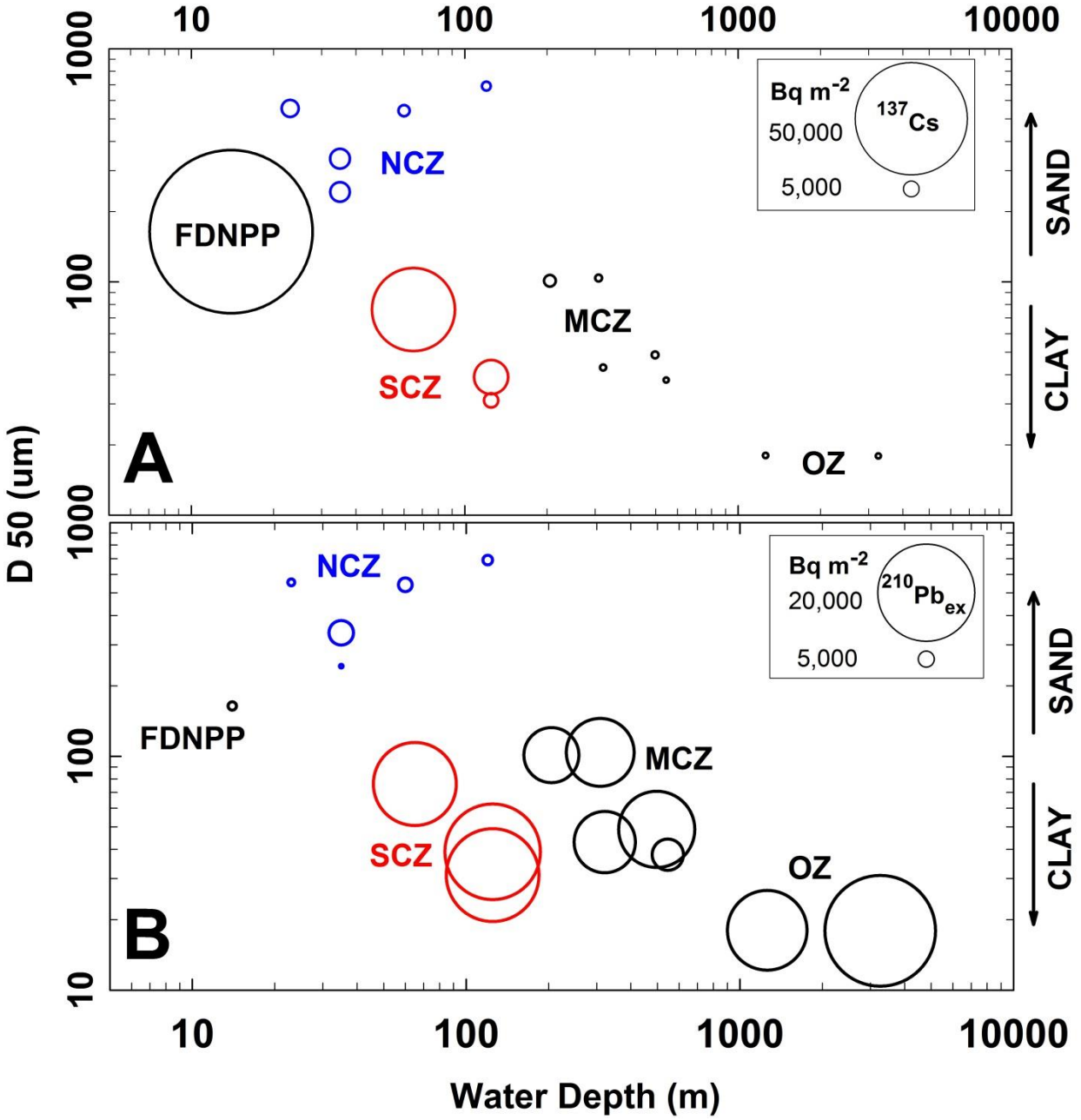

Black and Buesseler, Fig. 3

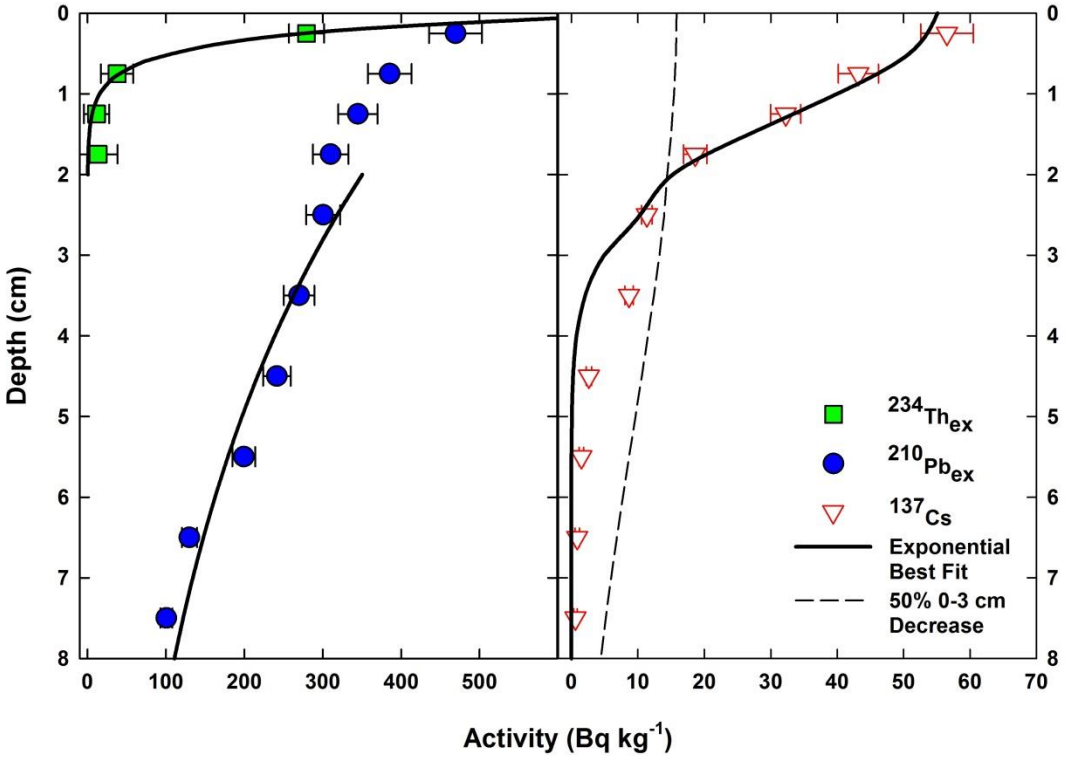

Black and Buesseler, Fig. 4

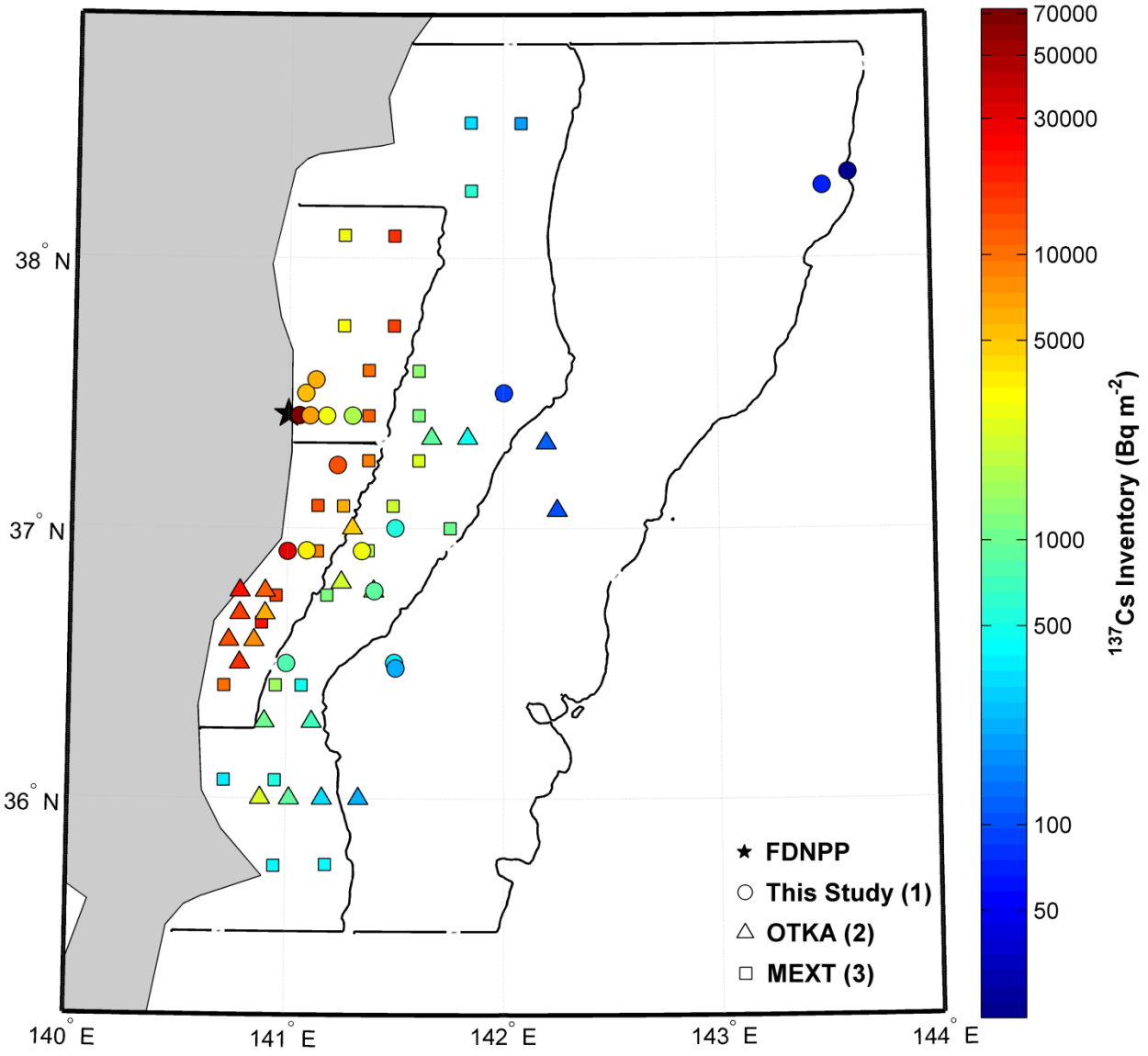

Black and Buesseler, Fig. 5

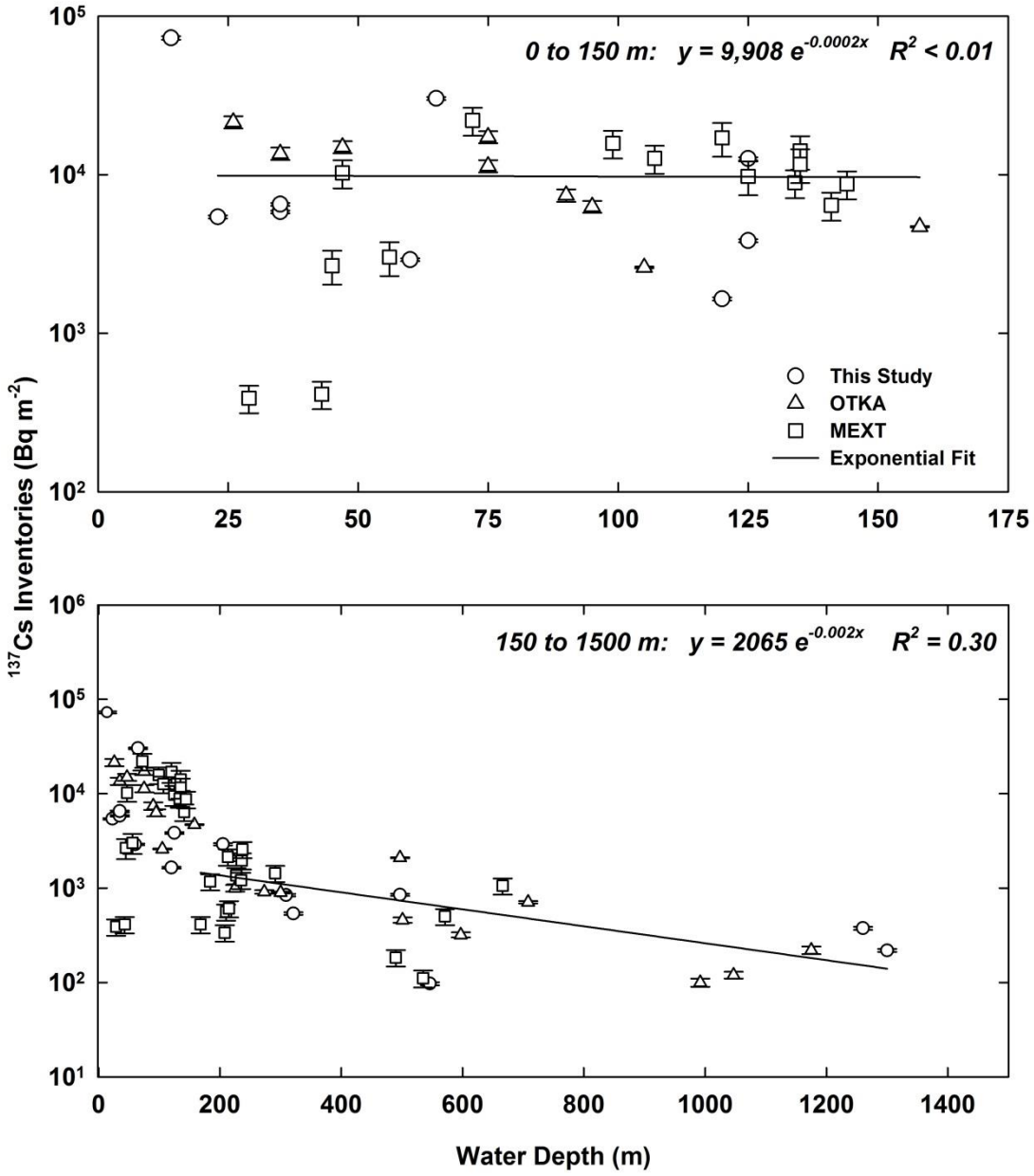

Black and Buesseler, Fig. 6